Characterization of the Product Radical Structure in the Co^{II}-Product Radical Pair State of Coenzyme B_{12}-Dependent Ethanolamine Deaminase by Using Three-Pulse ^2H ESEEM Spectroscopy†

Kurt Warncke*

Department of Physics, N201 Mathematics and Science Center, 400 Dowman Drive, Emory University, Atlanta, Georgia 30322

Received August 20, 2004; Revised Manuscript Received November 29, 2004

ABSTRACT: Molecular structural features of the product radical in the Co^{II}-product radical pair catalytic intermediate state in coenzyme B_{12}- (adenosylcobalamin-) dependent ethanolamine deaminase from *Salmonella typhimurium* have been characterized by using X-band three-pulse electron spin-echo envelope modulation (ESEEM) spectroscopy in the disordered solid state. The Co^{II}-product radical pair state was prepared by cryotrapping holoenzyme during steady-state turnover on excess 1,1,2,2-$^2H_4$-aminoethanol or natural abundance, $^1H_4$-aminoethanol. Simulation of the $^2H/^1H$ quotient ESEEM (obtained at two microwave frequencies, 8.9 and 10.9 GHz) from the interaction of the unpaired electron localized at C2 of the product radical with nearby ^2H nuclei requires four types of coupled ^2H, which are assigned as follows: (a) a single strongly coupled (effective dipole distance, $r_{eff} = 2.3$ Å) ^2H in the C5′ methyl group of 5′-deoxyadenosine, (b) two weakly coupled ($r_{eff} = 4.2$ Å) ^2H in the C5′ methyl group, (c) one ^2H coupling from a β-^2H bonded to C1 of the product radical (isotropic hyperfine coupling, $A_{iso} = 4.7$ MHz), and (d) a second type of C1 β-^2H coupling ($A_{iso} = 7.7$ MHz). The two β-^2H couplings are proposed to arise from two C1−C2 rotamer states of the product radical that are present in approximately equal proportion. A model is presented, in which C5′ is positioned at a distance of 3.3 Å from C2, which is comparable with the C1−C5′ distance in the Co^{II}-substrate radical pair intermediate. Therefore, the C5′ methyl group remains in close (van der Waals) contact with the substrate and product radical species during the radical rearrangement step of the catalytic cycle, and the C5′ center is the sole mediator of radical pair recombination in ethanolamine deaminase.

Ethanolamine deaminase (also known as ethanolamine ammonia-lyase) is a bacterial enzyme that catalyzes the coenzyme B_{12}- (adenosylcobalamin-) dependent conversion of aminoethanol **1** to acetaldehyde **4** and ammonia (*1*). It is a member of the family of coenzyme B_{12}-dependent enzymes (*2*−*5*), which use radical chemistry to catalyze 1,2-shifts of carbon (class I, carbon skeleton mutases) (*6*) and amino groups (class III, aminomutases) (*7*), and a 1,2-shift followed by elimination of an amino or hydroxyl group (class II eliminases, including ethanolamine deaminase) (*8*). The first step in all of the reactions is the cleavage of the cobalt−carbon bond of the coenzyme to form two $S = {}^1/_2$ species, low spin Co^{II} and the 5′-deoxyadenosyl radical, as depicted in the minimal catalytic mechanism in Figure 1. In ethanolamine deaminase, the C5′ carbon of the 5′-deoxyadenosyl radical abstracts a hydrogen atom (step HT1) from C1 of aminoethanol (*9*, *10*), forming the substrate radical **2** with unpaired electron spin density localized at C1 (*11*, *12*). The substrate radical rearranges to a product radical **3**, in which unpaired spin resides on C2 (*13*). Following rearrangement, the 5′-methyl group of 5′-deoxyadenosine returns a hydrogen atom to the product radical to form a diamagnetic product species, which regenerates the 5′-deoxyadenosyl radical. The cobalt−carbon bond is re-formed (*14*), and product is released from the enzyme to complete the catalytic cycle. The aim of the present study is to gain insight into the molecular mechanism of catalysis by using high-resolution pulsed-electron paramagnetic resonance (EPR[1]) spectroscopy to characterize structural features of the Co^{II}-product radical pair state in the ethanolamine deaminase from *Salmonella typhimurium*.

EPR spectroscopy is an incisive technique for characterizing the molecular structure of the radical pair intermediates in coenzyme B_{12}-dependent enzyme reactions (*15*). In ethanolamine deaminase, the Co^{II}-substrate radical state was shown to accumulate in high yield during steady-state turnover on the substrate, (*S*)-2-aminopropanol (*11*). Low-temperature EPR studies of this trapped state (*11*) and simulations of the EPR line shape (*16*) showed that Co^{II} and C1 were separated by the relatively large distance of 10−12 Å. Examination of the substrate radical in the presence of isotopic labeling of the C5′-methyl group by using pulsed-electron−nuclear double resonance (ENDOR) (*9*) and electron spin-echo envelope modulation (ESEEM) (*10*) revealed

† Supported by Grant R01 DK54514 from the National Institute of Diabetes and Digestive and Kidney Diseases of the National Institutes of Health.

* Tel: (404) 727 2975. Fax: (404) 727 0873. E-mail: kwarncke@physics.emory.edu.

[1] Abbreviations: EPR, electron paramagnetic resonance; ESEEM, electron spin-echo envelope modulation; ENDOR, electron−nuclear double resonance.

10.1021/bi048196t CCC: $30.25
Published on Web 02/12/2005

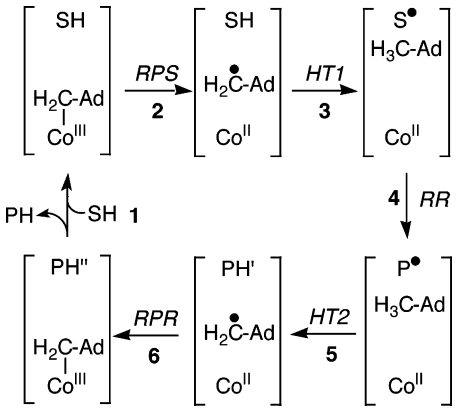

FIGURE 1: Minimal mechanism of catalysis for vitamin B_{12} coenzyme-dependent ethanolamine deaminase (*2*, *4*). The forward direction of reaction is indicated by arrows. The reaction is reversible for the substrate, (*S*)-2-aminopropanol (*49*, *63*, *64*). For the substrate, aminoethanol, step 4 and possibly step 3 are detectably irreversible (*13*, *63*, *65*, *66*). The steps are (1) product release/substrate binding, (2) radical pair separation (RPS), (3) hydrogen atom transfer 1 (HT1), (4) radical rearrangement (RR), (5) hydrogen atom transfer 2 (HT2), (6) radical pair recombination (RPR). Substrate-derived species are designated SH (bound substrate), S• (substrate radical), P• (product radical), PH′ and PH″ (bound product species), and PH (released products). The 5′-deoxyadenosyl β-axial ligand is represented as Ad-CH_2− in the intact coenzyme, and as Ad-CH_2• (5′-deoxyadenosyl radical) or Ad-CH_3 (5′-deoxyadenosine) following cobalt−carbon bond cleavage. The cobalt ion and its formal oxidation states are depicted, but the corrin ring and α-axial ligand of the coenzyme are not shown for clarity.

that the C5′−C1 distance was 3.2−3.3 Å. This closest-contact positioning indicates that C5′ is the mediator of radical migration from the cobalt to the substrate site (*9*, *10*). Orientation-selection ESEEM of the Co^{II}-substrate radical pair state revealed the three-dimensional arrangement of Co^{II}, the C5′-methyl group, and C1, and showed that the radical migration occurred over 6 ± 1 Å in the active site (*17*). In contrast to the Co^{II}-substrate radical pair state, the separation distance and orientation of C2 and the C5′-methyl group in the Co^{II}-product radical pair state have not been reported. Here, the first description of these mechanistically significant structural features of the product radical state is presented.

Scheme 1

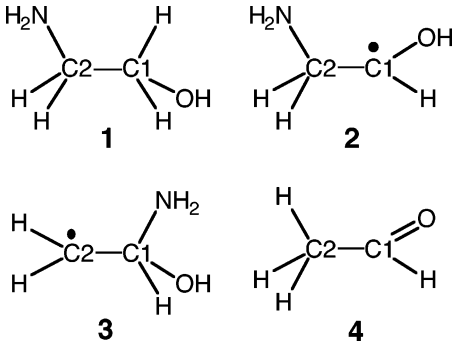

The Co^{II}-product radical pair state accumulates during steady-state turnover on the native substrate, aminoethanol, and is stabilized for low-temperature spectroscopy by cryotrapping (*13*). EPR simulation analyses lead to values for the Co^{II}−C2 distance in the Co^{II}-product radical pair of *S. typhimurium* ethanolamine deaminase of 9.7 ± 0.3 Å (*18*) and 9.3 Å (range, 8.5−10.5 Å) (J. M. Canfield and K. Warncke, unpublished). These distances are comparable with the reported Co^{II}−C1 separation distances in the Co^{II}-substrate radical pair state of 10−12 Å in Clostridium SP ethanolamine deaminase (*16*), and with values reported for the *S. typhimurium* enzyme of 11.1 Å (range, 10.9−11.5 Å) (*17*) and 11.0 Å (range, 10.2−11.9 Å) (*12*). Differences in the EPR line shape of the product radical generated from ^{14}N or ^{15}N-labeled aminoethanol evinced a carbinolamine (1-aminoethan-1-ol-2-yl) structure **3** (*19*). The radical rearrangement step therefore proceeds by the amine migration pathway, in which the amine nitrogen migrates from C2 to C1 to form **3** (*19*).

For the present studies, the product radical was cryotrapped during steady-state turnover on the deuterated substrate, 1,1,2,2-$^2H_4$-aminoethanol ($^2H_4$-aminoethanol), or on natural abundance, $^1H_4$-aminoethanol. The magnetic interactions of the unpaired electron at C2 with ^2H nuclei were then measured by using the three-pulse (stimulated-echo) ESEEM technique (*20*−*22*). The three-pulse ESEEM technique offers higher spectral resolution than the two-pulse ESEEM used previously for the substrate radical (*10*), which was advantageous for assignment of the multicomponent product radical spectra. Three general classes of ^2H nucleus are present in the cryotrapped product radical state. The multiple turnovers (≥300) of the enzyme prior to sample cryotrapping result in the rapid and complete exchange of ^2H into all three sites of the C5′ methyl group of 5′-deoxyadenosine (*23*). Two equivalent α-^2H (bonded to C2) and one β-^2H (bonded to C1) are also expected from the product radical structure **3**. The strong α-^2H coupling (*24*) places it outside of the microwave pulse bandwidth detection limit of the ESEEM technique (*20*−*22*). However, in preliminary work, we have shown that β-^2H coupling is detected (*19*). Here, a thorough simulation analysis of the β-^2H interaction is presented, which includes three-pulse ESEEM data collected at two different X-band microwave frequencies/magnetic fields and at six values of the microwave pulse timing parameter, τ.

The simulation of the three-pulse ^2H ESEEM from the product radical leads to ^2H coupling assignments for the three C5′ ^2H and for two types of β-^2H, which represent two different C1−C2 rotamer populations in the enzyme active site. Models are presented, which include the product radical C1−C2 rotamer structures and the proposed distance of the C5′-methyl group from C2. The results provide insights into the molecular mechanism of the radical rearrangement and radical migration reactions in ethanolamine deaminase.

EXPERIMENTAL PROCEDURES

Enzyme Preparation. Enzyme was purified from the *Eschericia coli* overexpression strain incorporating the cloned *S. typhimurium* ethanolamine deaminase coding sequences (*25*) essentially as described (*26*), with the exception that the enzyme was dialyzed against buffer containing 100 mM HEPES (pH 7.5), 10 mM KCl, 5 mM dithiothreitol, 10 mM urea, and 10% glycerol (*27*). Enzyme activity was determined as described (*28*) by using the coupled assay with alcohol dehydrogenase/NADH. The specific activity of the purified enzyme with aminoethanol as substrate was 25−30 μmol/min/mg.

Sample Preparation. Adenosylcobalamin (Sigma Chemical Co.), 1,1,2,2-$^2H_4$-aminoethanol ($^2H_4$-aminoethanol; Cam-

bridge Isotope Laboratories, Inc.), and natural abundance aminoethanol ($^1H_4$-aminoethanol; Aldrich Chemical Co.) were purchased from commercial sources. The reactions were performed in air-saturated buffer containing 100 mM HEPES (pH 7.5), 10 mM KCl, and 5 mM dithiothreitol. Identical results were obtained with air-saturated and anaerobic samples. All manipulations were carried out on ice under dim red safe-lighting. The final concentration of enzyme was 10−15 mg/mL, which is equivalent to 20−30 μM for a holoenzyme molecular mass of 500000 g/mol (*26*). Adenosylcobalamin was added to 120−180 μM, which is stoichiometric with active sites. The active site/holoenzyme stoichiometry of 6 is based on adenosylcobalamin titration of substrate radical formation (K. Warncke, unpublished) and is in agreement with the value obtained by two separate methods (*29*, *30*).

The product radical was generated by using a procedure for fast cryotrapping of steady-state intermediate states in ethanolamine deaminase (*13*). The procedure for specific incorporation of ^2H into the hydrogen positions of the C5′ carbon in enzyme-bound adenosylcobalamin has been described in detail (*13*). Briefly, following mixing of the enzyme−substrate solution with adenosylcobalamin, the sample was loaded into a 4 mm o.d. EPR tube, and the tube was plunged into liquid nitrogen-chilled isopentane ($T \approx 130$ K) to trap the Co^{II}-product radical pair state. The total elapsed time from mixing to isopentane immersion was approximately 15 s. Turnover of the enzyme on $^2H_4$-aminoethanol leads to exchange of ^2H into the C5′ hydrogen positions of the coenzyme within several turnovers (*23*). Under typical conditions (15 s trapping time, turnover number (k_{cat}) per active site of approximately 20 s^{-1}), an average of ≥300 turnovers were executed per active site.

ESE-EPR Spectroscopy. ESE-EPR spectra were collected by using a laboratory-designed and constructed wideband pulsed-EPR spectrometer that will be described elsewhere (K. Warncke, in preparation). The reflection microwave probe (*31*) incorporates a folded half-wave resonator (*32*). ESE-EPR spectra were obtained by using the two-pulse ($\pi/2-\tau-\pi$, where τ is the dephasing time) microwave pulse sequence (*20*−*22*).

ESEEM Spectroscopy. Data Acquisition and Processing. ESEEM was collected by using the three-pulse ($\pi/2-\tau-\pi/2-T-\pi/2$, where T is the waiting time) microwave pulse sequence (*20*−*22*), with microwave pulse-swapping and phase-cycling (*33*, *34*). The pulse-swapping sequence allows acquisition of envelope modulation that starts at the dead time limit of the spectrometer, which results in enhanced spectral resolution and reduced distortion in the Fourier transform of the ESEEM. The τ values were selected to eliminate envelope modulation from the multitude of distant, weakly dipolar-coupled solvent and protein "matrix" (*35*) protons that surround the radical. For the matrix ^1H, the hyperfine frequencies ν_α and ν_β, corresponding to the $m_s = +1/2$ (or α) and $m_s = -1/2$ (or β) electron spin manifolds, are both approximately equal to the free ^1H frequency, ν_{1H}, of 13.3 MHz at 313.0 mT (16.5 MHz at 388.8 mT). Suppression of matrix proton modulation occurs at $\tau = n/\nu_{1H}$, where $n = 1, 2, 3, \ldots$ (*36*, *37*).

Envelope modulation was dead time-reconstructed (*38*) and cosine Fourier transformed to generate ESEEM frequency spectra. When required, envelope modulation was also processed prior to Fourier transformation by removing the 40−60 ns amplitude trough in the pulse-crossover segment centered at τ. All data processing and analysis was performed with routines written in Matlab (Version 5, Mathworks, Natick, MA) and run on Macintosh computers.

ESEEM Simulations. Computational Approach. The coupled electron−nuclear spin system of the product radical was described by the following stationary-state spin Hamiltonian (*39*, *40*):

$$\hat{H} = \beta_e \hat{S}\cdot\mathbf{g}_e\cdot\boldsymbol{B}_0 + h\hat{S}\cdot\mathbf{A}\cdot\hat{I} - g_n\beta_n B_0\cdot\hat{I} + \hat{I}'\cdot\mathbf{Q}\cdot\hat{I}' \quad (1)$$

where g_e, β_e, and g_n, β_n are the electron and nuclear g-value and magneton, respectively, $\mathbf{g}_e$ is the electron g-tensor, $\boldsymbol{B_0}$ is the external magnetic field vector, h is Planck's constant, **A** is the hyperfine interaction tensor, **Q** is the nuclear quadrupole interaction tensor, and the $\hat{S}$ and $\hat{I}$ are electron and nuclear spin operators. In the strong field approximation assumed here, the electron Zeeman interaction is given by $g_e\beta_e B_0\hat{S}_z'$ where $\hat{S}_z'$ is the fictitious spin operator (*41*). The ESEEM waveform was simulated by direct implementation of the density matrix formalism of Mims (*36*, *42*). Details of the simulation analysis procedures, and justification for the application of the Hamiltonian in eq 1 to the radical in weakly coupled Co^{II}-radical pair states in ethanolamine deaminase, have been described (*39*, *40*). The simulated ESEEM incorporated the same dead time as the data, and it was dead time-reconstructed and processed in exactly the same way as the experimental ESEEM. ESEEM simulations were also performed with routines written in Matlab.

Adjustable and Fixed Simulation Parameters. In the ESEEM simulations, the variable input parameters include the following: The diagonal hyperfine tensor, $[A_{xx}, A_{yy}, A_{zz}]$, which is the sum of an isotropic component (A_{iso}) and an axially symmetric dipolar tensor, $[-A_{dip}, -A_{dip}, 2A_{dip}]$, where $A_{dip} = g_e\beta_e g_n\beta_n h^{-1} r_{eff}^{-3}$ (MHz), and r_{eff} is the effective distance separating the unpaired electron and nuclear spins. The single parameter, r_{eff}, thus determines the dipolar hyperfine tensor. For ^2H coupling, nuclear quadrupole interaction parameters represent the magnitude of the interaction (quadrupole coupling constant, e^2qQ/h), the asymmetry of the electric field gradient (asymmetry parameter, η), and Euler angles, $[\alpha, \beta, \gamma]$, which define the mutual orientation of the nuclear quadrupole and hyperfine tensor principal axes. The free electron and nuclear frequencies are fixed by the experimental magnetic field value. A compendium of ^2H nuclear quadrupole coupling parameters (*43*) shows that the e^2qQ/h and η values for ^2H bonded to carbon in different molecules are comparable, with typical values of approximately 0.12 MHz and 0.0−0.1, respectively. Therefore, fixed $e^2qQ/h = 0.12$ MHz and $\eta = 0.1$ were used. As found previously (*10*, *17*), variation of the Euler angles did not significantly influence the simulations for $r_{eff} \leq 3.0$ Å, but did for $r_{eff} > 3.0$ Å. The Euler angles relating the nuclear quadrupole and hyperfine tensors were therefore poorly constrained for $r_{eff} < 3.0$ Å and were fixed at $\alpha = \beta = \gamma = 0°$, corresponding to the case of coincident hyperfine and nuclear quadrupole interaction principal axes. For $r_{eff} > 3.0$ Å, β was varied in the simulations.

The variable parameters were adjusted, and the best match of the simulated and experimental time and frequency domain data was determined by visual scrutiny of overlaid data and

Table 1: ^{2}H Hyperfine Coupling Parameters and Relative Number of Coupled ^{2}H Used in the ESEEM Simulations[a]

^{2}H coupling	A_{iso} (MHz)	r_{eff} (Å)	rel. no.
^2H_s	−0.9 (0.4)	2.3 (0.1)	1.0[b]
$^2H_{\beta a}$	4.7 (0.3)	2.5 (0.1)	0.52 (0.04)
$^2H_{\beta b}$	7.7 (0.1)	2.4 (0.0)	0.48 (0.04)
^2H_w	−0.2 (0.0)	4.2 (0.0)	2.0[b]

[a] Mean values (standard deviations in parentheses) are presented for six simulations (τ = 300, 525, 975 ns at B_0 = 313.0 mT; τ = 303, 424, 787 ns at B_0 = 388.0 mT). [b] The relative number of ^2H_s and ^2H_w was fixed at 1.0 and 2.0, respectively.

simulations for each individual waveform or Fourier transform. The parameter values and uncertainties presented in Table 1 represent the mean and standard deviation of the parameters for the six different τ and B_0 conditions. The limits on the parameters represent values that, if exceeded, led to significantly poorer reproduction of the experimental data. Figures S2−S4 in Supporting Information show the results of variation of the individual hyperfine coupling parameters by ±10% from their best-fit values.

Combination of ESEEM from Multiple Hyperfine Couplings. When N nuclear spins are coupled to the same unpaired electron spin, the three-pulse envelope modulation is given by the sum of the product of the envelope modulation of the N individual hyperfine couplings, taken separately over the α and β electron spin manifolds, as follows (*37*, *44*):

$$E_{tot}(\tau,T) = \frac{1}{2}[\prod_i^N E_{\alpha,i}(\tau,T) + \prod_i^N E_{\beta,i}(\tau,T)] \qquad (2)$$

Here, $E_{tot}(\tau,T)$ is the τ- and T-dependent total envelope modulation, and $E_{\alpha,i}(\tau,T)$ and $E_{\beta,i}(\tau,T)$ are the modulation functions for hyperfine coupling with nucleus i in the α or β electron spin manifold, respectively. The modulation from each coupled electron-multinuclear spin system in a disordered sample contributes additively to the total modulation.

For the simulation of the ESEEM from the ^{2}H and ^{1}H product radical samples, the total modulation was first calculated by using the exact expression (eq 2), with terms in i representing the following four coupled hydrogen nuclei (H), which are assigned as described in the Discussion section: i = 1, H_s; i = 2, H_{w1}; i = 3, H_{w2}; i = 4, $H_{\beta a}$ or i = 4′, $H_{\beta b}$. The relative population of active sites with $H_{\beta a}$ was given by the fraction f [corresponding to i = 1, 2, 3, 4 where N = 4]. The relative population of active sites with $H_{\beta b}$ was given by the fraction 1 − f [corresponding to i = 1, 2, 3, 4′ where M = 4′]. The corresponding ESEEM from the ^{2}H and ^{1}H samples was separately calculated by using the following expression:

$$E_{tot}(\tau,T) = \frac{f}{2}[\prod_i^N E_{\alpha,i}(\tau,T) + \prod_i^N E_{\beta,i}(\tau,T)] + \frac{(1-f)}{2}[\prod_i^M E_{\alpha,i}(\tau,T) + \prod_i^M E_{\beta,i}(\tau,T)] \qquad (3)$$

The individually simulated $E_{tot}(\tau,T)$ waveforms corresponding to the ^{2}H and ^{1}H labeling were divided to obtain the ^{2}H/^{1}H quotient ESEEM.

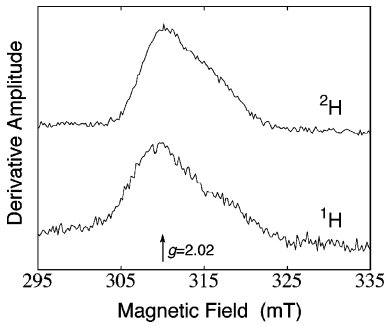

FIGURE 2: Two-pulse ESE-detected EPR spectra of the product radical in the Co^{II}-product radical pair state cryotrapped in ethanolamine deaminase. The product radical was generated by using $^2H_4$-aminoethanol (top) or natural abundance ($^1H_4$-) aminoethanol (bottom). The arrow corresponds to the position of ESEEM collection at g = 2.02 for the magnetic field value of 313.0 mT in Figures 3 and 4A. Amplitudes are normalized by scaling the ^{1}H spectrum by a factor of 3.1. Conditions: temperature, 6 K; τ, 400 ns; microwave frequency, 8.7680 GHz; microwave pulse power, 10 W; microwave pulse width, 20 ns; pulse sequence repetition rate, 500 Hz; 64 repetitions averaged per point; average of four (^{2}H) or seven (^{1}H) individual spectra.

In the experimental ESEEM, modulation from nuclei other than the ^{2}H and ^{1}H nuclei that undergo isotope exchange can be attenuated by dividing the modulation collected for the ^{2}H-labeled sample by the modulation collected for a ^{1}H, natural isotope abundance sample prepared under identical conditions (*37*, *45*). Division of three-pulse envelopes has previously proven successful in eliminating, by reducing to below the noise level, the contributions of common coupled nuclei to quotient ^{2}H/^{1}H three-pulse ESEEM (*45*−*47*). Features that allow the ^{2}H modulation to dominate the quotient ESEEM are as follows: (a) The modulation from coupling to natural abundance nuclei other than ^{1}H is weak in the product radical samples (*40*). (b) The strong matrix ^{1}H signal present in both ^{2}H and ^{1}H samples is suppressed by choice of the pulse timing parameter, τ, as described above. (c) For the exchangeable hydrogen sites, the ^{1}H line widths in the frequency domain are greater than the corresponding ^{2}H line widths by a factor of 6.51 (*24*), which is the ratio of the nuclear gyromagnetic ratios for ^{1}H and ^{2}H. Therefore, in the time domain, the bulk of the coupled ^{1}H modulation decays within the dead time of the pulsed-EPR spectrometer (*48*), and therefore does not make a significant contribution to the ESEEM, or the Fourier transform of the ESEEM.

RESULTS

EPR Spectroscopy. Figure 2 displays ESE-detected powder EPR spectra of the product radical intermediate cryotrapped during turnover on $^2H_4$-aminoethanol or $^1H_4$-aminoethanol in ethanolamine deaminase. The amplitudes of the spectra in Figure 2 are normalized, which requires multiplication of the ^{1}H spectrum by a factor of 3.1. The larger absolute spectral amplitude of the ^{2}H sample arises from the ^{1}H/^{2}H isotope effect of 4−6 on the steady-state rate-limiting second hydrogen transfer step (HT2; see Figure 1) (*1*, *49*) (L. E. Anderson and K. Warncke, unpublished). This leads to a greater steady-state accumulation of product radical in the ^{2}H sample. The difference in the line widths [full width at half-maximum (fwhm)] between the ^{2}H and ^{1}H spectra is 0.8 mT, which agrees well with the value of 0.7 mT reported

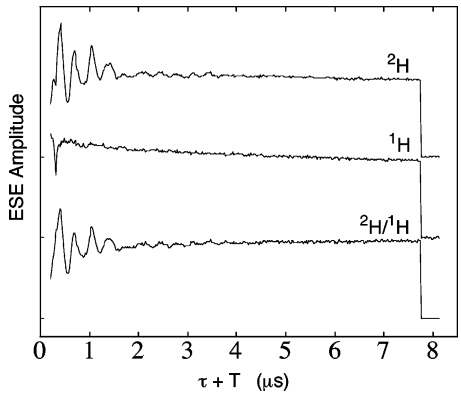

FIGURE 3: Experimental three-pulse ^{2}H, ^{1}H, and quotient ^{2}H/^{1}H ESEEM collected from the product radical in the Co^{II}-product radical pair intermediate that was generated by using the $^2H_4$- and $^1H_4$-labeled substrate radical in ethanolamine deaminase. The vertical axis is proportional to the integrated area of the electron spin echo. (Top) ESEEM from enzyme pretreated with $^2H_4$-aminoethanol. (Middle) ESEEM from enzyme pretreated with natural abundance ($^1H_4$-) aminoethanol. (Bottom) Quotient ESEEM. Conditions: temperature, 6 K; microwave frequency, 8.8585 GHz (^{2}H) and 8.8655 (^{1}H); magnetic field, 313.0 mT; microwave pulse power, 25−32 W; initial τ value, 160 ns; τ increment, 20 ns; $\pi/2$ pulse width, 20 ns; pulse repetition rate, 320 Hz; 64 repetitions averaged per point; average of 4 envelopes.

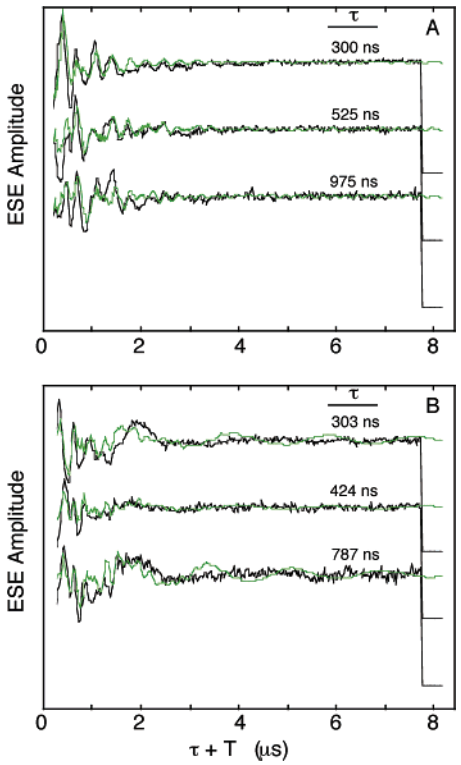

FIGURE 4: Experimental ^{2}H/^{1}H quotient three-pulse ESEEM collected from the product radical in the Co^{II}-product radical pair intermediate in ethanolamine deaminase (black), and overlaid ESEEM simulations (green). The ESEEM corresponds to three different values of τ at two values of microwave frequency/magnetic field. Simulation parameters are presented in Table 1. (A) B_0 = 313.0 mT; τ = 300, 525, and 975 ns. (B) B_0 = 388.0 mT; τ = 303, 424, and 787 ns. Conditions: temperature, 6 K; microwave frequency, 8.8585 GHz (^{2}H) and 8.8655 (^{1}H) for B_0 = 313.0 mT (g = 2.02), or 10.890 GHz for B_0 = 388.0 mT (g = 2.01); microwave pulse power, 25−32 W; initial τ value, 160 ns; τ increment, 20 ns; $\pi/2$ pulse width, 20 ns; pulse repetition rate, 320 Hz; 64 repetitions averaged per point; average of 4 envelopes.

earlier from continuous-wave EPR measurements (*40*). The amplitude of the broad resonance arising from Co^{II} is most prominent in the $g_\perp$ region at $g \approx 2.2$ (*50*) (corresponding to approximately 285 mT at the microwave frequency of 8.768 GHz), and is therefore not observed in the spectral region around $g = 2.0$ that is shown in Figure 2.

The difference in line widths indicate that hydrogen nuclei that are relatively strongly coupled to the unpaired electron spin undergo ^{2}H/^{1}H exchange. Incorporation of ^{2}H for ^{1}H at a site that participates in a hydrogen hyperfine interaction would result in a narrowing of the line shape, because of the reduction in nuclear gyromagnetic ratio by a factor of 6.51 for ^{2}H relative to ^{1}H (*24*). The ^{2}H/^{1}H isotope effects are expected to arise from strong coupling to the two α-H positions at C2, and possibly the β-H position on C1. The line width difference is relatively small, because the dominant line broadening of the radical spectrum arises from the electron−electron dipolar interaction and the enhanced relaxation of the radical by Co^{II} (*16*, *40*). Comparable, modest effects on the powder EPR line width of <1 mT have also been observed for hydrogen isotope substitutions on the substrate radical (*11*).

ESEEM Spectroscopy. ESEEM Waveforms. Figure 3 shows three-pulse ESEEM waveforms collected for the $^2H_4$- and $^1H_4$-aminoethanol-generated product radical. In the ESEEM experiment, the modulation of the echo envelope occurs with a periodicity corresponding to the inverse of the hyperfine (and nuclear quadrupole, for $I \geq 1$) frequencies of nuclear spins that are coupled to the unpaired electron spin (*36*, *51*). The top waveform in Figure 3 for the ^{2}H-labeled product radical shows a dominant modulation component with a period of approximately 300−500 ns, which is close to the reciprocal of the free deuteron frequency (ν_{2H}, 2.1 MHz) at the applied magnetic field of 313.0 mT. This modulation corresponds to ^{2}H nuclei that are coupled to the unpaired electron on C2. In contrast, the middle waveform in Figure 3 for the ^{1}H product radical shows extremely weak modulation that is close to the noise level. This is because the selected τ value suppresses the matrix ^{1}H modulation, and because the ^{1}H modulation corresponding to the ^{2}H modulation largely decays within the pulsed-EPR spectrometer dead time (see detailed description in Experimental Procedures).

The ^{2}H envelope modulation components can be enhanced relative to the modulation from hyperfine couplings that are common to each radical (*40*) by dividing the ^{2}H envelope (Figure 3, top) by the ^{1}H envelope (Figure 3, middle) (*37*, *45*). The envelope division also eliminates the rapid phase memory decay (T_m) of the echo for the $T < 0$ period, and attenuates the pulse-crossover artifact that occurs at coincidence of the second and third $\pi/2$ pulses ($T = 0$). The resulting quotient ESEEM, presented in Figure 3, bottom, is dominated by the ^{2}H modulation.

^{2}H/^{1}H quotient envelope modulation collected for the product radical at six different τ values and at two different values of the microwave frequency/magnetic field is shown in Figure 4. The selected magnetic field values of 313.0 and 388.0 mT correspond to the maximum amplitude of the ESE at the microwave resonator frequencies of 8.86 and 10.89 GHz. The presence of superposed contributions with different

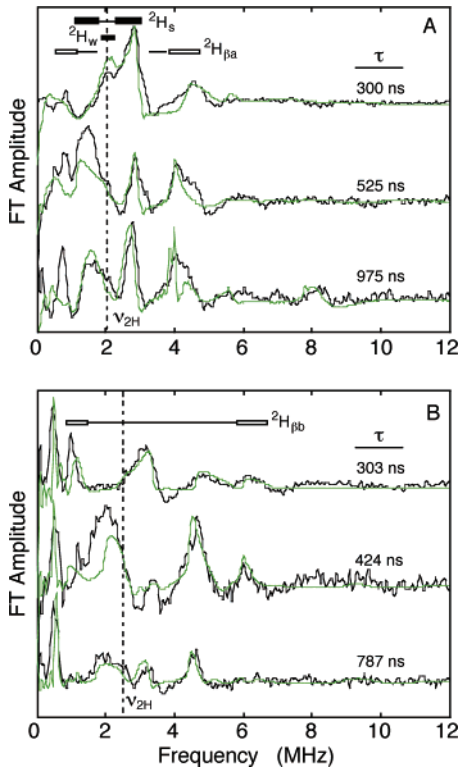

FIGURE 5: Cosine Fourier transforms of the three-pulse $^2H/^1H$ quotient ESEEM from the product radical in the Co^{II}-product radical pair intermediate in ethanolamine deaminase (black), and overlaid cosine Fourier tranforms of simulated ESEEM (green). The corresponding quotient ESEEM and ESEEM simulations are presented in Figure 4. Dashed lines mark the positions of the free deuteron resonance frequency (ν_{2H}), and hyperfine coupling assignments are shown. Experimental conditions are described in the Figure 4 caption, and simulation parameters are presented in Table 1.

periodicities suggests the contribution of more than one type of hyperfine-coupled ^2H to the modulation.

ESEEM Frequency Spectra. The quotient ESEEM shown in Figure 4 was cosine Fourier transformed to obtain the corresponding ESEEM frequency spectra presented in Figure 5. The spectra show a multicomponent line shape with intensity around the free ^2H frequency (ν_{2H}, 2.1 MHz at 313.0 mT; 2.5 MHz at 388.0 mT). All significant features at $\nu <$ 12 MHz correspond to ^2H hyperfine couplings, as shown by the characteristic increase in the resonance positions by 0.4 MHz when the magnetic field is increased from 313.0 to 388.0 mT.

The ^2H ESEEM line shapes shown in Figure 5 are composed of the following four sets of features: (1) A narrow line, which is most clearly revealed in the $\tau = 300$ ns spectrum in Figure 5A, is centered at the free ^2H frequency. This line arises from relatively weak ^2H coupling. (2) A broad line shape, with features that are split by approximately ± 0.8 MHz from ν_{2H}. This line shape arises from a relatively strong ^2H coupling. As shown in Figure 5, the relative amplitude of the split features is very sensitive to the τ value. The τ-dependence of the line shape is caused by the suppression effect (see description in Experimental Procedures: ESEEM Spectroscopy) (*37*, *42*). (3) The feature at 4.2−4.8 MHz (panel A, 313.0 mT) and 4.7−5.3 MHz (panel B, 388.0 mT) arises from a third type of ^2H coupling. The splitting of 2.1−2.7 MHz from ν_{2H} indicates a relatively large isotropic hyperfine coupling. The width of the feature is also consistent with a relatively strong dipolar hyperfine interaction. In support of this model, conjugate features are observed in the 0−1 MHz regions of the Fourier transforms in Figure 5 that correspond to the splitting in the other electron spin manifold. (4) A feature at relatively high frequency values of 5.8−6.4 MHz is clearly observed in the Fourier transforms obtained at 388.0 mT. This feature is also characterized by a relatively large isotropic hyperfine coupling, and the complexity of the spectral region from 0 to 1 MHz suggests the presence of a lower frequency conjugate to this high frequency feature. The features are weak (near to the noise level) in the 313.0 mT spectra. The increased amplitude at 388.0 versus 313.0 mT can be explained by the closer approach to the "exact cancellation" condition (*52*) for this coupling at the higher magnetic field value. This is because the spectrum corresponds to the case of $A > 2\nu_{2H}$ (where A is the hyperfine coupling), so that increasing magnetic field causes the low frequency hyperfine feature to shift to lower frequency, corresponding to the approach to a zero-field condition in the electron spin manifold corresponding to this transition. At the exact cancellation condition, the hyperfine and Zeeman magnetic fields at the coupled nucleus are equal in magnitude and opposite in direction for one electron spin manifold. A dramatic enhancement of the modulation amplitude occurs at and near the exact cancellation condition (*52*). This effect has been well-characterized for ^{14}N ESEEM (*37*, *52*, *53*).

DISCUSSION

Simulation of the $^2H/^1H$ Quotient ESEEM. ^2H Hyperfine Coupling Parameters. Figures 4 and 5 display the simulations of the quotient ESEEM and the corresponding Fourier transforms, respectively. The simulation parameters are collected in Table 1. The simulations of the time domain data in Figure 4 show good agreement with experiment in reproducing both the pattern and amplitude (depth) of the ^2H modulation, and the dependence of the pattern and amplitude on τ and B_0 values. The agreement is also reflected in the frequency domain simulations in Figure 5 by the presence of all hyperfine features for the different ^2H couplings, and by the reproduction of the relative amplitudes of the features from the different types of ^2H coupling. The assignment of the hyperfine coupling parameters to specific hydrogen sites is based on the following considerations: (a) a product radical structure in which the unpaired electron spin is localized on C2 and (b) analogies with the ^2H hyperfine couplings and line shapes in the Co^{II}-substrate radical pair state, which we have previously characterized by using ^2H ESEEM spectroscopy (*10*, *17*).

Coupling with C5′ Methyl Hydrogen Nuclei. The features in the range of $\nu_{2H} \pm 1.0$ MHz are assigned to the C5′ methyl ^2H nuclei. During turnover on $^2H_4$-aminoethanol, ^2H is rapidly exchanged into the C5′ hydrogen positions (*54*). Therefore, in the Co^{II}-product radical pair state, the C5′ methyl group of 5′-deoxyadenosine incorporates three ^2H nuclei. One of these nuclei is strongly coupled to the radical (^2H_s), as shown by the short $r_{eff} = 2.3$ Å and by the significant A_{iso} value of -0.9 MHz. This coupling gives rise to the split ^2H features nearest to ν_{2H}. The two additional ^2H on the C5′ methyl group can be accounted for by a longer range ($r_{eff} = 4.2$ Å) interaction (^2H_w). The coupling param-

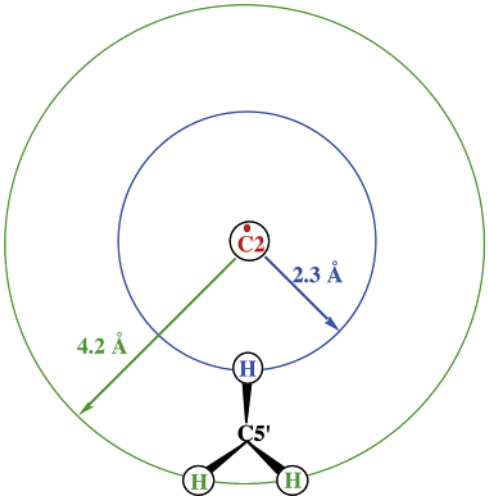

FIGURE 6: Cross-section through the model for the separation distances among C2 of the product radical, C5′ of 5′-deoxyadenosine, and the C5′-methyl group hydrogen atoms in the active site of ethanolamine deaminase in the Co^{II}-product radical pair state. The ESEEM results place the coupled ^2H_s and ^2H_w on spherical surfaces at the indicated radii from C2. The radii are consistent with the tetrahedral geometry and standard bond lengths for an sp^3-hybridized C5′ methyl group, which localizes the ^2H_s and ^2H_w nuclei as shown.

eters for ^2H_s and the ^2H_w are comparable with the values for the C5′ methyl ^2H coupling in the substrate radical (*10*, *17*), which were also characterized by a single strongly coupled ^2H ($r_{eff} = 2.2$ Å, $A_{iso} = -0.3$ MHz) and two weakly coupled ^2H ($r_{eff} = 3.8$ Å, $A_{iso} = 0$). Thus, the simulations place the coupled H_s and H_w nuclei on concentric spherical surfaces that are centered on C2, with radii of 2.3 Å and 4.2 Å, respectively. The separation distances among ^2H_s, the two ^2H_w, and C2 in the product radical are depicted in Figure 6. The C2−^2H distances are consistent with the tetrahedral substituent geometry of the sp^3-hybridized C5′ methyl group, if the C2−H_s−C5′ angle is approximately 150°. The model in Figure 6 therefore shows H_s and the two H_w localized to the C5′ methyl group.

Coupling with β-^2H Nuclei within the Product Radical. The two ^2H interactions with larger values of A_{iso} are assigned to interactions of the C2 unpaired electron spin density with ^2H bonded to C1 at the β-position, relative to C2 ($^2H_{\beta a}$, $^2H_{\beta b}$). The simulated spectra in Figure 5 reproduce the low intensity of the more strongly coupled $^2H_{\beta b}$ at 313.0 mT, and the emergence of the $^2H_{\beta b}$ amplitude at 388.0 mT. The r_{eff} values for the β-^2H couplings of approximately 2.4 Å are consistent with the expected C2-$^2H_\beta$ distance of 2.1−2.2 Å. Inspection of the product radical structure **3** in Scheme 1 shows that the presence of two β-^2H couplings is unexpected, because there is a single β-^2H nucleus at C1. Further, simulations incorporating a 1:2:1:1 stoichiometry of ^2H_s:^2H_w:$^2H_{\beta a}$:$^2H_{\beta b}$ gave β-^2H features in the Fourier transform that were too large (approximately 2-fold) compared to experiment, as shown in Figure S1, Supplementary Information. This suggested that each β-^2H was present in a 1:1 stoichiometry with ^2H_s. Therefore, simulations were performed assuming two populations of enzyme active sites, one with a 1:2:1 stoichiometry of ^2H_s:^2H_w:$^2H_{\beta a}$, and the other with a 1:2:1 stoichiometry of ^2H_s:^2H_w:$^2H_{\beta b}$. The relative populations of sites with the $^2H_{\beta a}$ coupling (fraction *f*) and sites with $^2H_{\beta b}$ coupling (fraction 1 − *f*) were varied (see eq 3). Successful

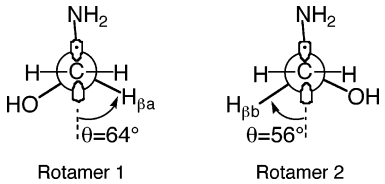

FIGURE 7: Proposed structure of the two observed product radical C1−C2 rotamers in the active site of ethanolamine deaminase in the Co^{II}-product radical pair state. For illustration, the 1-(*R*)-H_β and 1-(*S*)-H_β rotamers are arbitrarily assigned to $^2H_{\beta a}$ and $^2H_{\beta b}$ couplings, respectively.

simulations of the relative amplitudes of the C5′-^2H and β-^2H features were achieved for $f = 0.5-0.6$. We have previously presented evidence for two C1−C2 rotamer states, which was based on the simulation of only the $^2H_{\beta a}$ and $^2H_{\beta b}$ hyperfine features in the cosine Fourier transform of ESEEM collected at $\tau = 303$ ns, $B_0 = 388.0$ mT (*19*). The complete simulations shown in Figures 4 and 5, which include the ^2H stoichiometries and consistency of the hyperfine coupling parameters over all conditions, provide strong support for the model that the product radical exists in two different populations, characterized by two C1−C2 rotamer states.

Model for C1−C2 Rotamers of the Product Radical. The two C1−C2 rotamer states for the product radical are depicted in Figure 7. For the ESEEM simulations, it was assumed that identical ^2H_s and ^2H_w hyperfine couplings were present in each C1−C2 rotamer state. This corresponds to the same orientation of C5′ relative to C2 for each rotamer. However, each C1−C2 rotamer state includes only one type of β-^2H coupling, either $^2H_{\beta a}$ or $^2H_{\beta b}$. The Heller−McConnell expression (*55*) relates the value of A_{iso} for β-H coupling to the dihedral angle, θ, between the C−H_β bond and p-orbital axis on the coupling carbon atom, as follows:

$$A_{iso} = \rho B_2 \cos^2 \theta \qquad (4)$$

Here, B_2 is a constant equal to 24.9 MHz for ^2H (*56*) and ρ is the unpaired electron spin density at the coupling atom (C2). Substitution of the $^2H_{\beta a}$ and $^2H_{\beta b}$ A_{iso} values from Table 1 and assumed $\rho = 1$ into eq 4 leads to calculated dihedral angles of 64° and 56° for $^2H_{\beta a}$ and $^2H_{\beta b}$, respectively. The sum of the dihedral angles is 120°, which is the angular difference expected for the Newman projections between substituents on an sp^3-hybridized carbon atom. This observation is accounted for in the model by orienting the two rotamers so that $^2H_{\beta a}$ and $^2H_{\beta b}$ are positioned on opposite sides of the C1−C2 axis, as depicted in Figure 7. The ESEEM results are therefore consistent with the carbinolamine structure **3** for the product radical, which was proposed on the basis of the $^{14}N/^{15}N$ isotope effect on the product radical EPR line shape (*19*).

Figure 7 shows that the C1−N bond is essentially aligned with the partially filled p-orbital on C2 in the model for the product radical. In the substrate radical, the C2−N bond is aligned with the partially filled p-orbital on C1 (*1*, *12*). The essentially coparallel orientation of the C−N bonds with the partially filled p-orbitals in both the substrate and product radicals is also consistent with the amine migration rearrangement pathway.

Mechanisms of Formation of the Two Different C1−C2 Rotameric States. The two C1−C2 rotamer conformations originate from reorientation of the H−C1−O moiety by

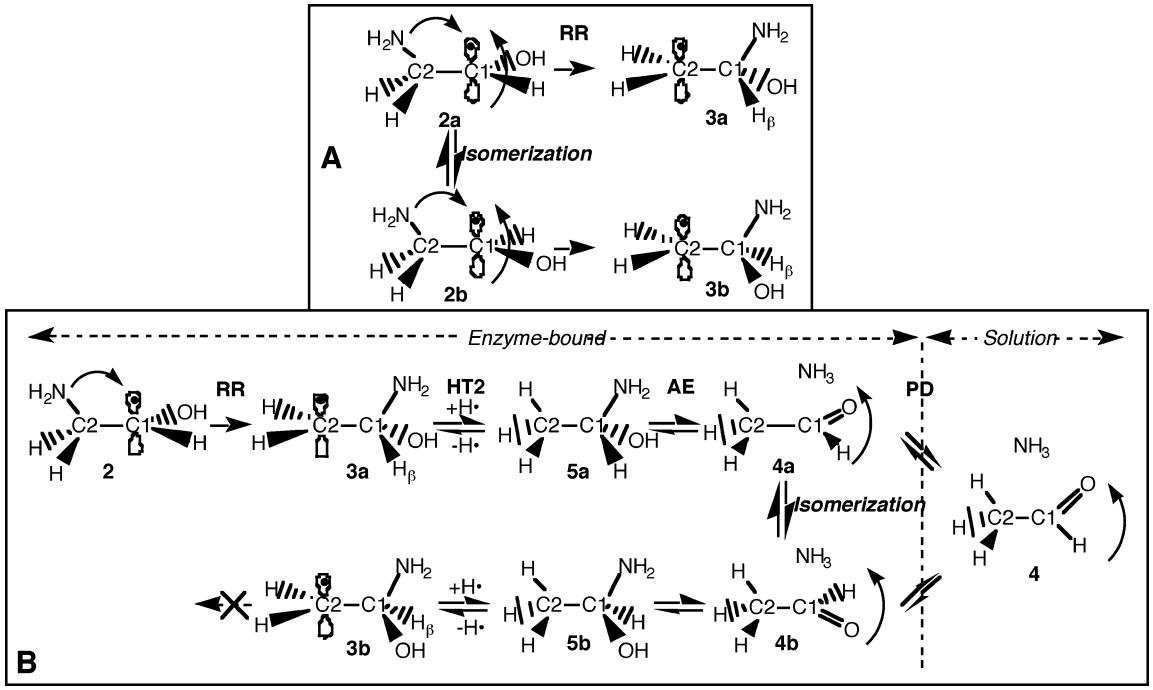

FIGURE 8: Possible mechanisms for the formation of the two observed C1−C2 rotamer states in the product radical in the active site of ethanolamine deaminase. The two mechanisms in panels A and B are distinguished by the steps in the catalytic sequence at which rotational isomerization of the H−C1−O group about the C1−C2 axis occurs. Active site topography and assumed single NH_2 (or NH_3) insertion path into the stereotopic H−C1−O center lead to the enantiomers **3a**, **3b** and **5a**, **5b**. Note that, for aminoethanol as substrate, the radical rearrangement (RR) step is detectably irreversible (*13*, *63*, *65*, *66*), whereas the hydrogen transfer (HT2), amine elimination (AE), and product dissociation (PD) steps are reversible (*62*). (A) Rotation of the H−C1−OH group occurs in the substrate radical state or during amine group migration, prior to product radical formation. The 1-(*R*)-H_β (**3a**) and 1-(*S*)-H_β (**3b**) sterioisomers of the product radical are formed directly following amine group migration. (B) Rotation of the H−C1═O group occurs in the product acetaldehyde. The sterioisomers **3a** and **3b** of the product radical are formed by the reverse of the HT2 hydrogen atom transfer step, following equilibration of the 1-*pro*-(*R*) (**4a**) and 1-*pro*-(*S*) (**4b**) product species with intermediate carbinolamine species **5a** and **5b**, respectively.

rotation about the C1−C2 bond, followed by stereoselective insertion of the amino group. There is precedent for rotation about the C1−C2 bond in catalytic intermediate states of ethanolamine deaminase. Rotation of the H−C2•−H methylene moiety about the C1−C2 axis prior to hydrogen atom transfer from C5′−H to C2• (HT2) has previously been demonstrated both for aminoethanol (*57*) and for (*R*)- and (*S*)-2-aminopropanol (*58*). As shown in Figure 8, there are two stages of the catalytic sequence where reorientation of the H−C1−O group relative to the amino group can occur. In the mechanism presented in Figure 8A, the trigonal H−C1•−OH moiety rotates prior to migrating NH_2 attachment at C1. Migration of NH_2 along the same physical path from C2 to C1 in the active site results in formation of 1-(*S*)-H_β and 1-(*R*)-H_β stereoisomers. In this mechanism, trigonalization of the C1 carbon following the first H atom abstraction (HT1, see Figure 1), and protein structural changes preceding or accompanying NH_2 migration, could create the conditions necessary for rotation of the H−C1•−OH moiety. An alternative mechanism, depicted in Figure 8B, is that the change in orientation of the H−C1═O plane relative to the NH_3 group occurs following formation of the product aldehyde. This mechanism involves an equilibrium among the states that follow the product radical state in the forward direction of the catalytic sequence. The H−C1═O reorientation could take place within the active site, or following dissociation and reassociation of the products.

The aldehydic H−C1═O reorientation mechanism in Figure 8B is favored over the carbinol radical H−C1•−OH reorientation mechanism in Figure 8A by the results of previous studies. $^1H/^2H$ kinetic isotope effects on the reaction of aminoethanols that were stereospecifically labeled with ^2H at the 1-(*R*) and 1-(*S*) positions indicate a favored abstraction of hydrogen in step HT1 from the 1-*pro*-(*S*) position (*59*, *60*), and this is consistent with transfer of ^3H from [5′-^{3}H]adenosylcobalamin to the 1-*pro*-(*S*) position of 2-aminopropanols (*58*). These studies imply binding and preferred orientation of the OH group of aminoethanol by the protein, at least in the bound substrate state. Flexibility in the H−C1•−OH orientation also does not appear well-suited for the "push−pull" mechanism that was proposed on the basis of theoretical calculations of the rearrangement energetics by Radom's group (*61*). This mechanism requires a specific hydrogen bonding interaction of a protein (or bound water) base with the −OH group to facilitate the migration of NH_2. In contrast, equilibration of free product (acetaldehyde and ammonia) with the product radical state has been demonstrated by the ammonia-dependent exchange of ^3H between the acetaldehyde C2 methyl hydrogen sites and the C5′ methyl hydrogen sites (*62*). These considerations lead to the proposal that H−C1−O reorientation is most likely to occur in the aldehyde state.

The rotational freedom may arise in part from a weakened binding interaction of the aldehydic oxygen atom with the site in the late stages of the reaction sequence, possibly owing to the loss of hydrogen bond donor capability present in the preceding −OH group. It is speculated that this would enhance product dissociation from the active site region.

Implications for the Mechanisms of the Radical Rearrangement and Radical Migration Reactions in Ethanolamine Deaminase. The model in Figure 6 indicates that the separation distance between C2 and C5′ in the product radical state is 3.3 Å, which represents closest (van der Waals) contact of the two carbon centers. The close contact of C2 and C5′ indicates that C5′ is the sole mediator of radical pair recombination (re-formation of intact adenosylcobalamin) following HT2. The closest contact distance of 3.2−3.3 Å between C5′ and C1 in the substrate radical state (*9*, *10*, *17*) indicated that C5′ is the sole mediator of radical pair separation in ethanolamine deaminase (*9*, *10*, *17*). Therefore, it is now well established that the C5′ center of the 5′-deoxyadenosyl moiety is the radical shuttle between cobalt in cobalamin and the substrate/product binding site.

The short, comparable C2−C5′ and C1−C5′ distances in the product radical and substrate radical states, respectively, suggest that the C5′ center remains in close contact with the substrate/product radical species throughout the rearrangement reaction. The intimate association of the C1−C5′−C2 hydrogen exchange triad would minimize atom-shift contributions to the activation energy for the rearrangement and hydrogen atom transfer reactions. The positioning of C5′ close to C1−C2 may also sterically restrict the physical path of the migrating amino group to the opposite side of the C1−C2 frame.

ACKNOWLEDGMENT

We thank Ms. Lori Anderson for technical assistance, Professor Dale E. Edmondson (Emory University) for use of fermentation facilities, and Dr. Jeffrey M. Canfield for critical reading of the manuscript.

SUPPORTING INFORMATION AVAILABLE

Figure S1: Comparison of simulations for two active site populations and for one active site population. Figure S2, Figure S3, and Figure S4: Simulations for individual variation of hyperfine coupling parameters by ±10% relative to the best-fit values. Figure S4: Simulations for a single H_w and in the absence of H_w coupling. This material is available free of charge via the Internet at http://pubs.acs.org.

REFERENCES

1. Bandarian, V., and Reed, G. H. (1999) in *Chemistry and Biochemistry of B12* (Banerjee, R., Ed.) pp 811−833, John Wiley and Sons, New York.
2. Frey, P. (1990) *Chem. Rev. 90*, 1343−1357.
3. Stubbe, J., and van der Donk, W. (1998) *Chem. Rev. 98*, 705−762.
4. Banerjee, R. (1999) *Chemistry and Biochemistry of B12*, John Wiley and Sons, New York.
5. Banerjee, R., and Ragsdale, S. W. (2003) *Annu. Rev. Biochem. 72*, 209−247.
6. Buckel, W., and Golding, B. T. (1996) *Chem. Soc. Rev. 25*, 329−338.
7. Frey, P. (2001) *Annu. Rev. Biochem. 70*, 121−148.
8. Toraya, T. (2003) *Chem. Rev. 103*, 2095−2127.
9. Lobrutto, R., Bandarian, V., Magnusson, O. T., Chen, X., Schramm, V. L., and Reed, G. H. (2001) *Biochemistry 40*, 9−14.
10. Warncke, K., and Utada, A. S. (2001) *J. Am. Chem. Soc. 123*, 8564−8572.
11. Babior, B. M., Moss, T. H., Orme-Johnson, W. H., and Beinert, H. (1974) *J. Biol. Chem. 249*, 4537−4544.
12. Bandarian, V., and Reed, G. H. (2002) *Biochemistry 41*, 8580−8588.
13. Warncke, K., Schmidt, J. C., and Ke, S.-C. (1999) *J. Am. Chem. Soc. 121*, 10522−10528.
14. Licht, S. S., Lawrence, C. C., and Stubbe, J. (1999) *J. Am. Chem. Soc. 121*, 7463−7468.
15. Gerfen, G. J. (1999) in *Chemistry and Biochemistry of B12* (Banerjee, R., Ed.) pp 165−195, John Wiley and Sons, New York.
16. Boas, J. F., Hicks, P. R., Pilbrow, J. R., and Smith, T. D. (1978) *J. Chem. Soc., Faraday Trans. 2 74*, 417−431.
17. Canfield, J. M., and Warncke, K. (2002) *J. Phys. Chem. B 106*, 8831−8841.
18. Ke, S.-C. (2003) *Biochim. Biophys. Acta 1620*, 267−272.
19. Warncke, K., and Canfield, J. M. (2004) *J. Am. Chem. Soc. 126*, 5930−5931.
20. Dikanov, S. A., and Tsvetkov, Y. D. (1992) *Electron Spin Echo Envelope Modulation (ESEEM) Spectroscopy*, CRC Press, Boca Raton, FL.
21. Deligiannakis, Y., Louloudi, M., and Hadjiliadis, N. (2000) *Coord. Chem. Rev. 204*, 1−112.
22. Schweiger, A., and Jeschke, G. (2001) *Principles of pulse electron paramagnetic resonance*, Oxford University Press, New York.
23. Bandarian, V., and Reed, G. H. (2000) *Biochemistry 39*, 12069−12075.
24. Wertz, J. E., and Bolton, J. R. (1986) *Electron Spin Resonance*, Chapman and Hall, New York.
25. Faust, L. P., Connor, J. A., Roof, D. M., Hoch, J. A., and Babior, B. M. (1990) *J. Biol. Chem. 265*, 12462−12466.
26. Faust, L. P., and Babior, B. M. (1992) *Arch. Biochem. Biophys. 294*, 50−54.
27. Harkins, T., and Grissom, C. B. (1995) *J. Am. Chem. Soc. 117*, 566−567.
28. Kaplan, B. H., and Stadtman, E. R. (1968) *J. Biol. Chem. 243*, 1787−1793.
29. Hollaway, M. R., Johnson, A. W., Lappert, M. F., and Wallis, O. C. (1980) *Eur. J. Biochem. 111*, 177−188.
30. Bandarian, V., and Reed, G. H. (1999) *Biochemistry 38*, 12394−12402.
31. Britt, R. D., and Klein, M. P. (1987) *J. Magn. Reson. 74*, 535−540.
32. Lin, C. P., Bowman, M. K., and Norris, J. R. (1985) *J. Magn. Reson. 65*, 396−374.
33. Fauth, J.-M., Schweiger, A., Braunschweiler, L., Forrer, J., and Ernst, R. R. (1986) *J. Magn. Reson. 66*, 74−85.
34. Fauth, J.-M., Schweiger, A., and Ernst, R. R. (1989) *J. Magn. Reson. 81*, 262−274.
35. Hyde, J. S., Rist, G. H., and Eriksson, L. E. G. (1968) *J. Phys. Chem. 72*, 4269.
36. Mims, W. B. (1972) *Phys. Rev. B 5*, 2409−2419.
37. Mims, W. B., and Peisach, J. (1989) in *Advanced EPR: Applications in Biology and Chemistry* (Hoff, A. J., Ed.) pp 1−57, Elsevier, New York.
38. Mims, W. B. (1984) *J. Magn. Reson. 59*, 291−306.
39. Ke, S.-C., Torrent, M., Museav, D. G., Morokuma, K., and Warncke, K. (1999) *Biochemistry 38*, 12681−12689.
40. Ke, S.-C., and Warncke, K. (1999) *J. Am. Chem. Soc. 121*, 9922−9927.
41. Abragam, A., and Bleaney, B. (1970) *Electron Paramagnetic Resonance of Transition Ions*, Clarendon Press, Oxford.
42. Mims, W. B. (1972) *Phys. Rev. B 6*, 3543−3546.
43. Hellwege, K.-H., and Hellwege, A. M. (1988) *Landolt-Bornstein Numerical Data and Functional Relationships in Science and Technology*, Vol. a, Springer-Verlag, New York.
44. Dikanov, S. A., Shubin, A. A., and Parmon, V. N. (1981) *J. Magn. Reson. 42*, 474−487.
45. Mims, W. B., Davis, J. L., and Peisach, J. (1990) *J. Magn. Reson. 86*, 273−292.
46. Warncke, K., and McCracken, J. (1994) *J. Chem. Phys. 101*, 1832−1841.
47. Warncke, K., and McCracken, J. (1995) *J. Chem. Phys. 103*, 6829−6840.
48. Astashkin, A. V., Dikanov, S. A., and Tsvetkov, Y. D. (1987) *Chem. Phys. Lett. 136*, 204−208.
49. Babior, B. M. (1982) in *B12* (Dolphin, D., Ed.) pp 263−387, Wiley, New York.
50. Pilbrow, J. R. (1982) in *B12* (Dolphin, D., Ed.) pp 431−462, Wiley, New York.
51. Rowan, L. G., Hahn, E. L., and Mims, W. B. (1965) *Phys. Rev. 137*, A61−A71.

52. Mims, W. B., and Peisach, J. (1978) *J. Chem. Phys. 69*, 4921−4930.
53. Flanagan, H. L., and Singel, D. J. (1987) *J. Chem. Phys. 87*, 5606−5616.
54. Bandarian, V., Poyner, R. R., and Reed, G. H. (1999) *Biochemistry 38*, 12403−12407.
55. Heller, C., and McConnell, H. M. (1960) *J. Chem. Phys. 32*, 1535−1539.
56. Fessenden, R. W., and Schuler, R. H. (1963) *J. Chem. Phys. 39*, 2147.
57. Retey, J., Suckling, C. J., Arigoni, D., and Babior, B. M. (1974) *J. Biol. Chem. 249*, 6359−6360.
58. Diziol, P., Haas, H., Retey, J., Graves, S. W., and Babior, B. M. (1980) *Eur. J. Biochem. 106*, 211−224.
59. Gani, D., Wallis, C. O., and Young, D. W. (1983) *Eur. J. Biochem. 136*, 303−311.
60. Yan, S.-J., McKinnie, B. G., Abacherii, C., Hill, R. K., and Babior, B. M. (1984) *J. Am. Chem. Soc. 106*, 2961−2964.
61. Wetmore, S. D., Smith, D. M., Bennet, J. T., and Radom, L. (2002) *J. Am. Chem. Soc. 124*, 14054−14065.
62. Carty, T. J., Babior, B. M., and Abeles, R. H. (1971) *J. Biol. Chem. 246*, 6313−6317.
63. Carty, T. J., Babior, B. M., and Abeles, R. H. (1974) *J. Biol. Chem. 249*, 1683−1688.
64. Graves, S. W., Fox, J. A., and Babior, B. M. (1980) *Biochemistry 19*, 3630−3633.
65. Babior, B. M. (1969) *J. Biol. Chem. 244*, 449−456.
66. Weisblat, D. A., and Babior, B. M. (1971) *J. Biol. Chem. 246*, 6064−6071.

BI048196T